LIDAR measurements during Aerosols99

Kenneth J. Voss[1], Ellsworth J. Welton[2], Patricia K. Quinn[3,4], James Johnson[3,4], Anne Thompson[5], and Howard R. Gordon[1]

(1) Department of Physics, University of Miami, Miami, Fl.

(2) SSAI, NASA-GSFC, Code 912, Greenbelt, Md.

(3) Pacific Marine Environmental Laboratory, NOAA, Seattle, Wa.

(4) Joint Institute for the Study of Atmosphere and Ocean, University of Washington, Seattle,Wa.

(5) Atmospheric Chemistry and Dynamics Branch, NASA/Goddard Space Flight Center, Greenbelt, Md.

Running title: LIDAR during Aerosols99

*Corresponding author email address: voss@physics.miami.edu

GAP index numbers: 0305, 0649, 0315, 3360, 9325

Submitted J. Geophysical Res., 6/29/00, Aerosols99 Special Section

Abstract

The Aerosols99 cruise took place during the period from January 14, to February 8 1999 on the R/V Ron Brown. The cruise track was almost a straight line from Norfolk, Va. to Cape Town, South Africa and afforded the opportunity to sample several different aerosol regimes over the North and South Atlantic. A Micro Pulse LIDAR system was used continually during this cruise to profile the aerosol vertical structure. Inversions of this data illustrated a varying vertical structure depending on the dominant air mass. In clean maritime aerosols in the Northern and Southern Hemispheres the aerosols were capped at 1 km. When a Dust event from Africa was encountered the aerosol extinction increased its maximum height to above 2 km. During a period in which the air mass was dominated by biomass burning from Southern Africa, the aerosol layer extended to 4 km. Comparisons of the aerosol optical depth derived from LIDAR inversion and surface sunphotometers showed an agreement within ± 0.05 RMS. Similar comparisons between the extinction measured with a nephelometer and particle soot absorption photometer (at 19 m altitude) and the lowest LIDAR measurement (75 m) showed good agreement (± 0.014 km^{-1}). The LIDAR underestimated surface extinction during periods when an elevated aerosol layer was present over a relatively clean surface layer, but otherwise gave accurate results.

1. Introduction

The Aerosols99 cruise took place during the period from January 14, to February 8 1999 on the R/V Ron Brown. The cruise track was almost a straight line from Norfolk, Va. to Cape Town, South Africa and afforded the opportunity to sample several different aerosol regimes over the North and South Atlantic. A multidisciplinary group participated on this cruise allowing for the measurement of an extensive suite of chemical, physical, and optical properties of the surface aerosol [Bates et al. this issue]. Along with these surface measurements a Micropulse LIDAR system [SESI, Burtonsville, MD] [Spinhirne et al., 1995] was operated continually to provide vertical profile information on the aerosol distribution. Ozonesondes and Radiosondes provided profiles of the temperature, humidity, and ozone distribution, which gave additional information on the structure of the atmosphere. Finally 5-day meteorological back trajectories provided information on the sources of the sampled aerosols. All of this information, when combined, gives a more complete picture of the aerosol structure over the Atlantic.

The cruise track presented a chance to look at many of the aerosol regimes over the Atlantic. This cruise track was impacted by aerosols from the North American continent, by Saharan Dust, by biomass burning on the African continent, and by clean maritime air in the regions between. There is very little information on the vertical distribution of the aerosols over the ocean, yet the vertical distribution of these aerosols can impact the accuracy of climate models and atmospheric corrections needed for retrieving ocean color. The Saharan Dust and biomass burning aerosols typically absorb

light. While atmospheric correction of ocean color imaging can be done for non-absorbing aerosols without knowledge of the aerosol vertical structure [Gordon, 1997)] the optical effect of absorbing aerosols is very dependent on the vertical structure [Gordon et al., 1997]. Aerosol models for atmospheric correction of ocean color imagery must account for this vertical structure when dealing with absorbing aerosols, yet there is little data available on this problem. This cruise offered an excellent opportunity to measure the aerosol vertical structure and have an extensive set of correlated measurements of the boundary layer aerosol.

In addition to atmospheric correction, it is important to have information on the vertical structure to understand how the surface measurements of the aerosol properties are related to the aerosols in the rest of the atmospheric column. A LIDAR gives direct information on the vertical distribution of aerosols. At times the surface measurements can be very different from the column above [Welton et al., 2000]. The LIDAR provides additional information that can be used to extend the surface measurements or show the presence of other layers above the surface.

During this cruise a micro pulse LIDAR [Spinhirne et al., 1995] was used to provide the vertical structure information. This LIDAR is a very compact system and was operated continuously during the cruise. With careful calibration and data reduction, accurate information on the aerosol vertical structure of the atmosphere can be obtained. This cruise allowed us to look at the relationship between the vertical structure of the aerosols, relative humidity (RH), temperature, surface physical and chemical aerosol properties, and back trajectories.

2 Methods

2.1 LIDAR

The Micropulse LIDAR [SESI, Burtonsville, MD] is a small compact LIDAR system which averages high repetition, low energy pulses to obtain a profile of attenuation/backscattering in the atmosphere [Spinhirne et al.,1995]. The Micropulse LIDAR used during the cruise operated at 523 nm, with a pulse repetition rate of 2500 Hz, the vertical resolution was 75m, and data was collected to 30 km. During the day the signal above 10 km became increasingly noisy due to a combination of attenuation in the boundary layer and background sunlight at 523 nm, but during the night low noise data could be obtained to 20 km in the absence of clouds. The details of the algorithm to retrieve the AOD and vertical profile of extinction or backscattering from the Micropulse LIDAR are detailed elsewhere [Welton, 1998, Welton et al., 2000b], however an overview of the technique will be presented here.

The basic equation governing LIDAR propagation, when the LIDAR is vertically oriented is:

$$Er(t) = CEo(\beta_r(180,z) + \beta_a(180,z))\exp(-2 * \int_0^z [c_r(z') + c_a(z')]dz') / z^2 \quad (1)$$

Where Er is the received energy, Eo is the outgoing pulse energy, $\beta_r(180,z)$ is the Rayleigh (molecular) backscattering, $\beta_a(180,z)$ is the aerosol backscattering, c_r is the Rayleigh attenuation, c_a is the aerosol attenuation, and C is an instrument calibration

constant. The time the signal is received is related to the altitude, z, by the time it takes for the LIDAR pulse to travel up to that altitude and back ($z = tc/2$, where c is the speed of light). By using time resolved return signals, profiles of the backscattering and attenuation can be obtained. C contains information on system parameters such as throughput, solid angle acceptance of the receiver, divergence of the laser beam and other parameters. While in principal this could be calculated [Spinhirne et al., 1980], in practice it is much simpler and more accurate to derive this parameter from measurements in the field, as will be discussed below. For a practical LIDAR system such as the MPL, there are other important effects which must be taken into account, namely the overlap and afterpulse functions. The overlap function describes the loss in signal strength at close range. Signal loss is due to optical design and to poor focusing to the detector by the MPL telescope at close range (less than 4 km). Signals at ranges greater than the overlap range are not effected by this problem. The afterpulse function is a result of cross-talk between the laser pulse and detector, as well as dark noise in the system. Both of these effects were corrected for in this data set in the manner described by Welton et al.[2000b].

When the AOD is known from independent measurements (such as with a handheld sunphotometer) the system calibration constant C can be determined [Welton et al., 2000b]. During cloud free periods during the cruise, episodic measurements of the AOD were made with a Microtops sunphotometer (Solar Light Co., Philadelphia, PA). For the LIDAR profile corresponding to the AOD measurement, a clean aerosol free layer above the boundary layer is found (for this cruise this was typically 6-7 km). This is usually obvious from the range corrected LIDAR signal by looking for a region for which

$\ln[Er(t)*z^2]$ is decaying at the rate appropriate for Rayleigh scattering. The returned energy from that altitude is simply:

$$Er(t) = CEo\beta_r(180,z)\exp(-2*\int_0^z [c_r(z') + c_a(z')]dz')/z^2 \tag{2}$$

Or

$$C = Er(t)z^2[Eo\beta_r(180,z)\exp(-2*AOD)\exp(-2*\int_0^z c_r(z')dz')]^{-1} \tag{3}$$

All of the factors on the right hand side of Eq. 3 are measured (AOD) or calculated, thus C can be determined. The calibration coefficient was fit to a linear equation and decreased linearly during the cruise by 20%.

Once the LIDAR calibration coefficient is determined, for each period a clean aerosol free layer above the boundary layer is found. With the calibration coefficient and this clean layer, the returned energy is given by Eq. 2 above, and Eq. 3 can be rewritten to obtain the AOD. It is important to note that this product does not depend on any assumption of the extinction/backscatter ratio. The accuracy of our calibration procedure is estimated to be ±3%. The accuracy of the AOD calculation is affected by this calibration coefficient, and the accuracy with which the overlap and afterpulse corrections were made. The accuracy of the AOD determined from the LIDAR is estimated to be ±0.02 in optical depth, but this error can increase due to other factors such as system noise.

With the AOD determined, an inversion must be made of the LIDAR return signal to obtain the extinction or backscattering profile. Since the LIDAR return depends on both the backscattering and extinction of the aerosols and molecules this leads to 4 variables to find from one input. The molecular (Rayleigh) backscatter and extinction coefficients can be calculated, reducing the unknowns. To reduce the number of free variables an assumption is made about the ratio between the extinction and backscatter coefficient, otherwise known as S (units are sr). We use a top-down inversion with a constant S for aerosols [Fernald et al., 1972, Fernald, 1984, Welton et al., 2000b], our exact method is described in detail in Welton [1998] and Welton et al.[2000b]. In this method the LIDAR equation is re-written in the form:

$$Er(t) = CEo(\beta_r(180,z) + c_a(z)/S_a)\exp(-2*\int_0^z [c_r(z') + c_a(z')]dz')/z^2 \quad (4)$$

Where S_a is S for aerosols. An inversion of the LIDAR return signal is performed, with an initial guess for S_a, to determine the profile of $c_a(z)$. This profile is then integrated and compared with the AOD obtained from Eq.. 3. S_a is adjusted with this result, and the procedure is iterated. This process is continued until the AOD and the integrated profile of $c_a(z)$ agree within 0.5%. Since S_a is assumed to be constant, $\beta_a(180,z)$ is just $c_a(z)/S_a$

The final accuracy of this inversion depends on the assumption of a constant S_a through the aerosol layer. With additional information this constraint could be removed, but without this errors are introduced. Even without changes in aerosol composition, changes in RH can effect S_a by changing the size distribution and index of refraction of

the aerosols [Ackermann, 1998]. The radiosonde data (discussed below) indicated that the variation in RH through the aerosol layer changed between the different regions along the cruise track(defined below). The constant S_a that is determined from the LIDAR inversion is a column averaged S_a. The errors introduced by this assumption will be discussed in more detail in the discussions of the individual regions and a comparison with the surface extinction measured with a nephelometer and a PSAP.

2.2 Radiosonde

Radiosondes, [Vaisala, RS80-15GH] were launched from the deck of the ship at 10:45 and 22:45 UTC each day. This launch time ensured that each radiosonde would be in the middle of its profile during the synoptic times of 0000 and 1200 UTC. The radiosondes measured vertical profiles of temperature, relative humidity, and horizontal winds. The winds were calculated from GPS measurements of the sonde horizontal position. Most radiosonde profiles extended to at least 15 km altitude. The sondes transmitted one data point every 10 seconds so that the raw data from the sondes (used here) had a vertical resolution of 20 to 40 meters.

To help define the variation of temperature with altitude, the rate of change of the temperature with altitude, $\Delta T/\Delta z$, was derived from the temperature data. $\Delta T/\Delta z$ (°C/km) was calculated by using a sliding five point least-squares-fit to the temperature data ($\pm$ 2 points around the specific altitude). This altitude interval is approximately 100-200 m.

2.3 Back-trajectories

Five day back-trajectories were made using the isentropic trajectory model at Goddard Space Flight Center/NASA [Schoeberl et al., 1992]. These trajectories were

initialized from the position of the ozonesonde launches along the cruise track. Clusters of back-trajectories were run from each launch to capture the uncertainties associated with analyzed winds (Numerical Center for Environmental Prediction (NCEP) 2.5 X 2.5 deg).

3 Results

The first discussion will compare LIDAR-derived AOD and extinction to AOD and extinction derived from independent measurements. We will then look at the overall LIDAR cruise data and investigate the results of the LIDAR and other vertical profile information for specific cruise regions.

3.1 AOD comparison

Voss et al. [this issue] shows the complete data set of AOD measurements obtained during the cruise, including the LIDAR measurements. This data set included a set of 3 Microtops Sunphotometers [Solar Light Co., Philadelphia, PA] independent of the one used to calibrate the LIDAR. To investigate the agreement between the LIDAR derived AOD and the sunphotometer AOD we grouped the LIDAR data and Sunphotometer data into common 72-minute measurement periods. In Fig. 1 the comparison between the two data sets are shown for all periods which have measurements with both techniques. The error bars for the sunphotometer measurement is the standard deviation of the distribution of sunphotometer measurements during the specific interval. The LIDAR error bars are due to the uncertainty in the LIDAR calibration constant, and signal noise (including afterpulse and overlap noise). The line in the figure is the 1:1 line. The agreement between the two methods is good, the RMS difference is 0.05 (optical depth). For larger

AOD the LIDAR AOD appears slightly higher than the sunphotometer AOD. The difference could be due to the LIDAR technique, to different measurement volumes (the LIDAR is vertical, the sunphotometer measures along the solar path), or differences in the specific measurement time in the 72 minute period. In general though the LIDAR derived AOD agrees with the standard sunphotometer technique to within the stated errors.

3.2 Surface extinction comparison

We did not have simultaneous measurements of the vertical extinction profile from an independent source (such as an aircraft) during this cruise, however we have done this in the past and compared this data with the LIDAR inversion with good results (Welton et al., 2000). During this cruise we had surface scattering and absorption measurements [Quinn et al., this issue] with which to compare the lowest altitude bin of the LIDAR. The aerosol was sampled at 19 m altitude with an integrating nephelometer (TSI Model 3563) and a particle soot absorption photometer (PSAP, Radiance Research). The scattering coefficient (measured at 55% RH and 550nm) was adjusted to ambient RH using the RH measured on the ship and previously measured f(RH) relationships. For the marine air mass regions, f(RH) for the light scattering coefficient was based on measurements during onshore flow at Cape Grim, Tasmania [Carrico et al., 1998]. In continentally-influenced regions f(RH) from continental air masses at Sable Island, Nova Scotia [McInnes et al., 1998] was used. For the light absorption coefficient (measured at 55% RH and 565 nm), f(RH) was assumed to equal one.

These surface extinction measurements were compared with the extinction retrieved from the LIDAR inversion at the lowest altitude bin (75 m). The comparison through the cruise is shown in Fig. 2. The agreement is generally very good, but there are specific regions for which the agreement is not as good. Figure 3 shows the comparison of the two measurements more quantitatively. The RMS difference between the two measurements was 0.014 km^{-1}. In this figure the measurements are broken into regions as defined later in the text (section 3.4). The most pronounced bias between the two measurements occurs during portions of Region 5 and at the beginning of Region 6 (to approximately 13° S). The extreme of this is near 5°-10° S when the surface values of the LIDAR are set to zero. During this period we had an elevated aerosol above a clean marine boundary layer (MBL) (MBL properties were determined from the surface chemistry measurements [Quinn et al., this issue]). In the portions of Region 5 (the lower surface extinction areas) and in Region 6a, the total column AOD did not decrease as much as the surface extinction did. When there is an elevated aerosol layer above a clean (or relatively clean) lower layer, the lidar inversion underestimates the extinction in the lower layer. It could also be that this difference is simply due to the different sampling altitudes and this effect is most important in this region. In general the LIDAR inversion worked well even in the near field, which has the most difficulties due to calibration difficulties. However, this analysis shows a case where the surface LIDAR data may be suspect because of the presence of an elevated aerosol layer over the relatively clean surface layer

3.3 LIDAR data through cruise

Figure 4 shows the contour plot of the extinction profile during the cruise. The contour plot is built from the LIDAR data, with 75m vertical resolution and at the data points marked at the bottom of the graph. Gaps in data were predominately due to clouds; however, during periods of high sun angle (solar noon) the LIDAR was turned off to avoid direct sunlight entering the detector (this also had to take into account possible ship roll, as direct sunlight would cause a complete failure of the system). Also delineated in the figure is the division into regions, discussed in detail below. As can be seen there was a large variation in both vertical structure and magnitude of the extinction, which was dependent on both location and recent meteorological transport.

While the aerosol obviously reached higher levels near the equator, it is also interesting to see how the aerosol is distributed, proportionately, for a given profile. Figure 5 shows a contour of the integrated extinction coefficient. This was calculated as:

$$IntegratedExtinction(z) = \frac{\int_{0}^{z} c_a(z')dz'}{\int_{0}^{6km} c_a(z')dz'} * 100 \qquad (5)$$

Once again the data points on which the contours were produced are shown at the bottom of the graph. Before 8 N and after 15 S, 25% and 50% lines (the altitude at which 25 and 50% of the AOD has been accounted for already) are fairly constant at 0.5 km and 0.8 km. The 75% and 90% lines, during this time, show periods for which more aerosol (relative to the rest of the column) was added at 1-1.5km (approximately 14 N and 20S). Between 8 N and 15S the surface layer is cleaner than the elevated layers. Thus all the contours rise during this period. In particular at the beginning of region 6 the 90% level

was the highest of the cruise. At this time there was a very clean lower level, and an elevated aerosol. While the optical depth [Voss et al, this issue] and extinction (Figure 4) were not maximum here, the clean lower level had the effect of making the upper aerosols a more important contribution to the column properties.

Figure 6 shows S_a derived from the LIDAR inversions through the cruise, also shown are the error bars on this derived parameter [method described in Welton et al., 2000b]. These will also be discussed in the specific regional discussions below, but the main feature is that during the periods of low total column extinction and low AOD, in regions 2 and late 6, S_a tended to have low values characteristic of maritime aerosols. During the periods of high AOD and high total column extinction, S_a was higher, typical of smaller particles and continental aerosols.

3.4 Specific regional vertical structure features

We will now discuss the differences in vertical structure of the lower atmosphere (<7 km) defined for the different regions. These regions were defined by surface trace gas concentrations, aerosol chemical and physical properties, and trajectories at the 500 m arrival height, [Bates et al., this issue], and may be somewhat different than those defined by other information with vertical profiles such as LIDAR or ozonesondes [Thompson et al. 2000]. The five day back-trajectories are shown in Fig. 7 and 8. The trajectories shown correspond to the weighted central point in each cluster at 1km and 4km levels. Time of trajectory initiation is 12Z with crosses marking every 24hr. For each region a typical radiosonde/LIDAR profile is shown. In each case the figure shows the radiosonde data (RH and $\Delta T/\Delta z$) along with the average of three LIDAR extinction coefficient

profiles obtained within 1 hour of the radiosonde profile. Because of intense clouds there are no LIDAR data for Region 1, so we begin our discussion with Region 2.

3.4.1 Region 2: Northern Hemisphere clean (31° N – 15.5° N)

In this region back trajectories at 1km and 4 km indicated that the airmass origin was over the North Atlantic (Figs. 7 and 8). Surface measurements of the aerosol chemistry indicated that the aerosol was clean maritime aerosol [Bates et al., this issue]. Example radiosonde and LIDAR profiles from this region (for DOY 18.5, N 27.7°) are shown in Figure 9.

In the example shown there is a strong temperature inversion at 1 km, and another at 2 and 4.5 km. The RH, in this example, stayed relatively constant at 80±10% up to 3 km. The aerosol was capped by the 1 km inversion, as witnessed by the LIDAR extinction coefficient. In general the extinction coefficient was low throughout this region (less than 0.2 km^{-1} peak), and the peak extinction coefficient was below 1 km, with very little extinction above 1 km (this example had the largest extinction above 1 km). The extinction profiles indicated that 90% of the AOD occurred below 2-3 km. The temperature structure seemed to vary, with strong inversions often occurring between 1-1.5 km. These temperature inversions were typically associated with the top of the aerosol layer. Relative humidity was generally above 80% throughout the aerosol layer.

Since the surface chemistry and back trajectories all indicated that this was a maritime atmosphere, there is no indications that there were drastic changes in aerosol composition in the aerosol layer. With the RH limited between 80 and 100%, Ackermann's model [Ackermann, 1998] for S_a for a maritime atmosphere, indicates that

the value should be approximately 25, with RH effects only indicating a range from 23-27. Thus our assumption of a constant S_a is a reasonable approximation in this region. We found that the S_a average for this region was 32±6 sr, which is near the values derived above. As discussed elsewhere [Voss et al, this issue] the AOD was low in this region (around 0.09±0.02) with a low angstrom exponent (0.27±0.27). The low angstrom exponent correlated with the low S_a indicating that the aerosol size distribution was weighted towards larger particles.

One final feature in this region was that initially the RH stayed high (>60%) throughout the column below 7 km. At 25° N the structure changed, becoming dryer above 3 km. By 23.7° N the humidity was less than 10% between 3 and 6 km, with some excursions above 10% occurring between 6 and 7 km. Since this was above the aerosol layer, there was no visible effect on the aerosol vertical structure. A more complete picture of the vertical profile of RH through the cruise is shown in Bates et al. [this issue].

3.4.2 Region 3: Dust (15.5° N – 8° N)

During the next portion of the cruise we had a significant dust event that changed the surface and vertical aerosol structure. Back trajectories at 1 km showed the aerosol source switching to the coast of Africa, with 4 km trajectories still coming from the North Atlantic.

A typical example of the vertical structure is shown in Fig. 10 for Day 24.5, N 11.2°. The radiosonde data throughout this period indicated a strong temperature inversion at 1.5 km and another temperature feature at 4-5 km. The RH was relatively

constant at 80-100% in the lower layer, below the 1.5 km temperature inversion. However at this inversion the RH decreased rapidly to 20-40%. The RH stayed constant at this level to the upper temperature feature (4-5 km) where it seemed to decrease to near 0%RH for a 1 km layer, after which it would increase back to 20-40%.

The LIDAR profile data showed two distinct layers, with a sharp minimum in extinction between them. The lower layer was capped by the temperature inversion at 1.5 km. The upper layer peaked at 2 km, with a subsequent gradual decrease with altitude. By 4 km the aerosol extinction was very low (<0.02 km^{-1}). The peak extinction in the lower layer was approximately 0.3 km^{-1}, while the peak extinction in the next layer was approximately 0.1 km^{-1}, so most of the AOD occurred in the lower layer. During this period, 90% of the AOD occurred below 2-3 km.

The column averaged S_a during this period was 41±8 sr. This is significantly higher than the S_a predicted by Ackermann (1998) for desert aerosols. Ackermann's work assumed spherical particles, however dust particles are often non-spherical which increases S_a by decreasing the backscattering at 180 degrees. This value for S_a agrees with earlier measurements by Welton et al. [2000]. In this region while the RH in each layer was relatively constant, the RH changed significantly between the upper and lower layer (80-100% to 40%). However because desert aerosol responds only weakly to RH, this change effects S_a very weakly (less than 10% change in S_a [Ackermann, 1998]). Thus changes in the S_a due to humidity are not expected. With the upper layer being very distinct, it is possible that a different aerosol was in the upper layer, however we have no in-situ chemical information on this layer to say what the layer might be. We also note that the earlier comparison in Fig. 3 showed no definite bias for this region. Thus the

constant S_a algorithm for the LIDAR inversion is the best we can use with the available information.

3.4.3 Region 4: Mixed Dust and Biomass burning (8° N – 3° N)

This period was characterized by the surface chemistry to be changing from the previous dust event to a biomass-burning aerosol. Back trajectories at 1 and 4 km indicated that the column aerosol was coming from Africa.

Radiosonde data indicated very strong and varying temperature and humidity structure through this period, and it is difficult to pick a representative profile. Figure 11 is an example of the structure during this period, for day 26, N 7.5°. In all of the radiosondes there was a strong temperature inversion near 1 km. At times there were other inversions above this with varying strength. The humidity was typically high (above 80%) below the lower inversion, but in the lower 7 km the RH decreased irregularly to 20-40%.

There was always a large LIDAR derived extinction peak near 1 km, with extinction values on the order of 0.3 km^{-1}. Additionally a peak occurred near 2 km with significant extinction (near 0.2 km^{-1}). The aerosols continued higher, with significant extinction to near 4 km. The 90% level for the AOD extinction was at 2.7 km, somewhat higher than in previous regions. The minimum between the lower and upper peak was not as distinct, or at as low an altitude, in this region as in the previous indicating there may have been more mixing between the layers.

The average S_a in this region increased to 52 $\pm$10 sr, which is between Ackermann's continental and desert aerosols, possibly reflecting the mix of aerosols at this location.

With the large peaks in aerosol extinction the AOD was significantly higher with the average AOD being 0.41. The angstrom exponent was also higher here, reaching 0.52, but because of clouds there were few sunphotometer measurements on which to base this angstrom exponent.

3.4.4 Region 5: Biomass burning (3° N – 5° S)

The next region reached during the cruise had surface aerosol chemistry characteristics of biomass burning. Back trajectories at 1km were mostly over the south Atlantic, however 4 km trajectories were from central Africa and the 8 km trajectories were also from the African coast.

Typical radiosonde and LIDAR data are shown in Fig. 12 and are from DOY 29, S 2.3°. In this region there were typically temperature inversions at 1.5 – 2 km, then other inversions above this (3, 4, 5 km and above). The RH varied between staying above 80% all the way to 4.5 km, to having a minimum of 40% at 2 km. It is difficult to find a general trend.

The aerosol extinction profile also varied over this region. In all cases significant aerosol extinction extended to 4 km. The 90% AOD level in this region averaged 3.3 km. The peak extinction reached >0.20 km^{-1}, with broad (>2 km) peaks. At times the peak moved off of the 1 km level to 2-3 km, but was typically at 1 km. The aerosol also seemed to decrease at 2 km, but then maintained a significant extinction to 4 km.

The S_a during this period was relatively high, 60$\pm$ 6 sr, which is a little lower than the value predicted for continental aerosol at this RH (>80%) by Ackermann[1998]. The average AOD was high, 0.36, with a very high average angstrom exponent of 0.882. This

indicates that the aerosol particles were probably relatively small, which agrees with the high measured S_a.

3.4.5 Region 6: Southern hemisphere clean (5° S – 24.5° S) and Region 7: South Atlantic temperate marine air mass (24.5° S – 33° S)

After going through these intense aerosol events, the surface chemistry again indicated a clean maritime situation [Bates et al., this issue]. Interestingly, while the surface measurements indicated a change at 5° S, the back trajectories did not switch as rapidly. The 1km trajectories were over the south Atlantic, however early in the Region (between 5° S and 12° S) 4 km trajectories were still over southern Africa and only switched to the south Atlantic after 12° S. An example of the earlier period is shown in Fig. 13, while an example of the later period is shown in Figure 14. Figure 13 is for Day 30.5, S 7.4°, while Fig. 14 is for Day 35.5, S 23.6°. We have grouped these two regions together, because the vertical structure of the late part of region 6 was basically the same as that of region 7.

The radiosonde data for the earlier period shows a strong temperature inversion at 1.5 km. The RH is typically very high (>80%) below this inversion, but decreases at the inversion to 50-60%. The aerosol extinction profile shows why the surface chemistry appeared clean, yet column AOD was not small. One can see that the surface extinction is below 0.01 km^{-1}, while the column extinction reaches >0.1 km^{-1} at 1 km or greater. During this early period, significant aerosol extended to 4 km, with the average 90% AOD level at 3.2 km, showing how high the aerosol was in the atmospheric column. The S_a in the early period was 63 ±12 sr, much higher than the values determined for the N.

Hemisphere clean region, and close to the value of the biomass burning. As can be seen in Figure 2 and the discussion above, the algorithm results are more uncertain when an optically dense upper layer is above a clean maritime layer. The algorithm tends to underestimate the extinction in the lower level. In terms of the overall column optics this is not a significant error, however it does underestimate the scattering in this lower level significantly.

By the end of the period the region resembles the Northern Hemisphere clean situation. The radiosondes show a strong inversion at approximately 1.5 km. The RH stays high (80-100%) to this altitude then drops to low values(30-40%) above the inversion. Aerosols are capped at 1 km by the inversion, but only reach extinction of 0.1 km^{-1} or so below the inversion and are at background (<0.01 km^{-1}) above the inversion. The 90%AOD level is at 1.4 km. The S_a also decreases to levels seen in the first region (36$\pm$16 sr). AOD and angstrom exponents are also down to the values in Region 2 (0.094 and 0.35 respectively [Voss et al., this issue]). The structure in these clean northern and southern hemisphere cases is the same.

4. Conclusions

With the LIDAR and associated measurements during this cruise we were able to determine the aerosol vertical structure of the lower portion (<7 km) of the atmosphere. Comparisons of the LIDAR derived AOD and extinction with sunphotometers and a surface nephelometer and PSAP showed that the LIDAR inversions were giving reasonable results throughout the cruise. Specific situations, particularly clean lower layers below elevated aerosol layers, caused the problems with the near field LIDAR

Quinn, P.K., D.J. Coffman, T.S. Bates, T.L. Miller, J.E. Johnson, K. Voss, E.J. Welton, and C. Neususs, Dominant aerosol chemical components and their contribution to extinction during the Aerosols99 cruise across the Atlantic, *J. Geophys. Res., submitted*, 2000.

Schoeberl, M. R., Lait, L.R., Newman, P. A., Rosenfield, J. E., The Structure of the Polar Vortex , *J. Geophys. Res.*, 97, 7859-7882 (1992).

Spinhirne, J.D., J.A. Reagan, and B.M. Herman, Vertical Distribution of Aerosol Extinction Cross Section and Inference of Aerosol Imaginary Index in the Troposphere by LIDAR Technique, *J. Appl. Meteorol.*, 19, 426-438 (1980).

Spinhirne, J. D., Rall, J., and V. S. Scott, Compact eye-safe LIDAR systems, *Rev. Laser Eng.*, 23, 26 – 32 (1995).

Welton, E. J. Measurements of Aerosol Optical Properties over the Ocean using Sunphotometry and LIDAR, Ph. D. Dissertation. University of Miami, Coral Gables, 1-150 (1998).

Welton, E. J., K. J. Voss, H. R. Gordon, H Maring, A. Smirnov, B. Holben, B. Schmid, J. M. Livingston, P. B. Russell, P. A. Durkee, P. Formenti, M. O. Andreae, Ground-based LIDAR Measurements of Aerosols During ACE-2: Instrument Description, Results, and Comparisons with other Ground-based and Airborne Measurements, *Tellus*, **52**: 635 – 651 (2000a).

Welton, E. J., J. R. Campbell, J. D. Spinhirne, and V. S. Scott, Aerosol and Cloud measurements using micropulse LIDAR systems, *J. Atmos. Oceanic Tech.* Submitted, (2000b).

Figure 6) S_a (extinction/backscattering) derived throughout the cruise. Vertical lines delineate regions as defined in Bates et al.[this issue]. S_a was lower in clean maritime airmasses then in those impacted by dust or biomass burning.

Figure 7) 1 km back-trajectories, Regions as discussed in text are shown divided by lines on the graph.

Figure 8) 4 km trajectories, Regions as discussed in text are shown divided by lines on the graph.

Figure 9) Radiosonde and LIDAR derived profiles typical for Region 2, Northern Hemisphere clean (31° N – 15.5° N). This specific case was for DOY 18.5, N 27.7°. LIDAR extinction is shown as the fine line with no symbols. This is an average of the nearest three profiles (each of which is a 10 minute cloudfree average) around the Radiosonde launch. Relative Humidity is displayed as the line marked with filled circles, while $\Delta T/\Delta z$ is displayed as the line marked with filled squares. Note overall extinction is low and capped by the first temperature inversion (positive $\Delta T/\Delta z$).

Figure 10) Radiosonde and LIDAR derived profiles typical for Region 3, Dust (15.5° N – 8° N). This specific case was for DOY 14.5, N 11.2°. Symbols are as in Figure 9. Extinction has increased from Region 2 and there is another aerosol layer above the first temperature inversion (positive $\Delta T/\Delta z$).

Figure 11) Radiosonde and LIDAR derived profiles typical for Region 4: Mixed Dust and Biomass (8° N – 3° N). This specific case was for DOY 26, N 7.5°. Symbols are as in Figure 9. Extinction is still high. The temperature, humidity and aerosol structure are all much more complicated than earlier in the cruise.

Figure 12) Radiosonde and LIDAR derived profiles typical for Region 5: Biomass burning (3° N – 5° S). This specific case was for DOY 29, S 2.3°. Symbols are as in Figure 9. Extinction is still high. Aerosol layer doesn't show a minimum between upper and lower layers.

Figure 13) Radiosonde and LIDAR derived profiles typical of the early portion of Region 6: Southern hemisphere clean (5° S – 24.5° S). This specific case was for DOY 30.5, S 7.4°. Symbols are as in Figure 9. Extinction is still high. This area was distinguished by having low surface extinction with an elevated aerosol layer with high extinction.

Figure 14) Radiosonde and LIDAR derived profiles typical of the later portion of Region 6: Southern hemisphere clean (5° S – 24.5° S) and Region 7: South Atlantic temperate marine air mass (24.5° S – 33° S). This specific case was for DOY 35.5, S 23.6°. Symbols are as in Figure 9. Extinction is now low again. This area is similar to the clean Northern Hemisphere case.

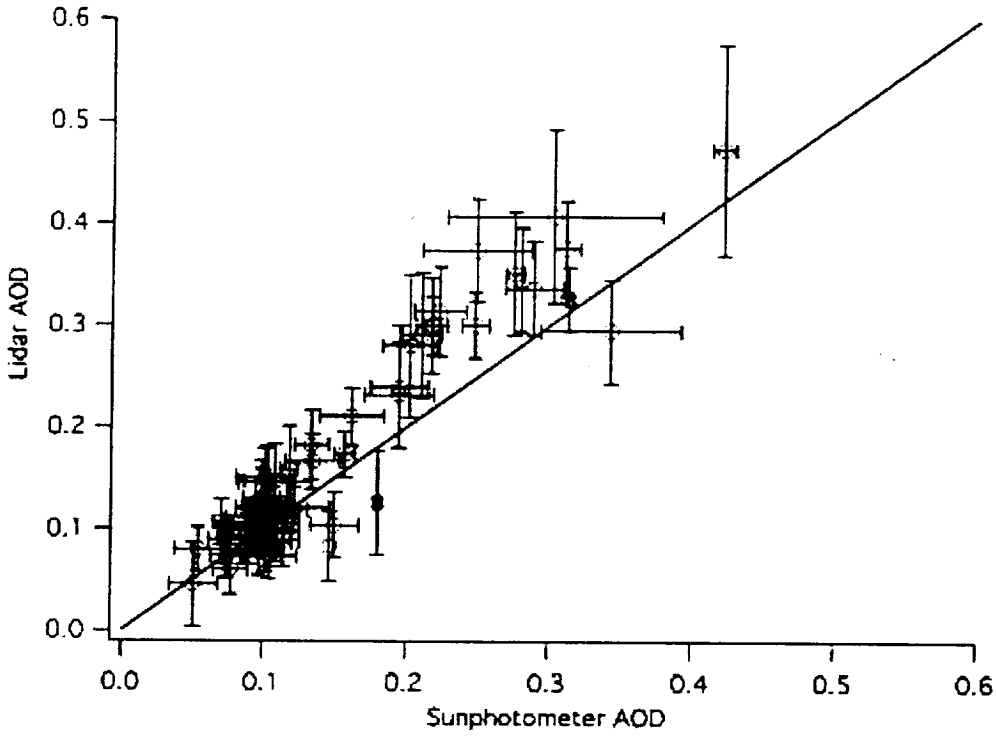
0.6
0.5
0.4
0.3
0.2
0.1
0.0
Lidar AOD
0.0
0.1
0.2
0.3
0.4
0.5
0.6
Sunphotometer AOD

Figure 1

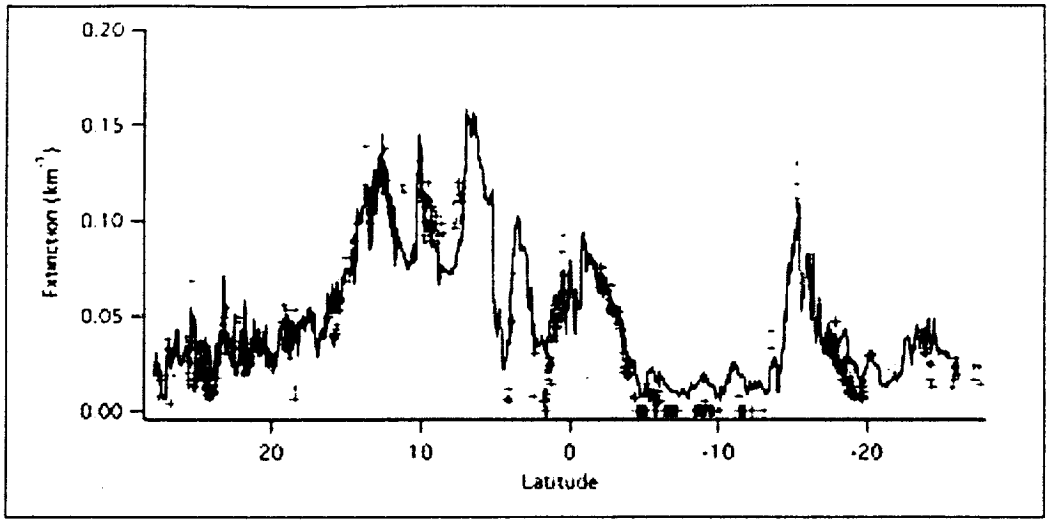

Figure 2

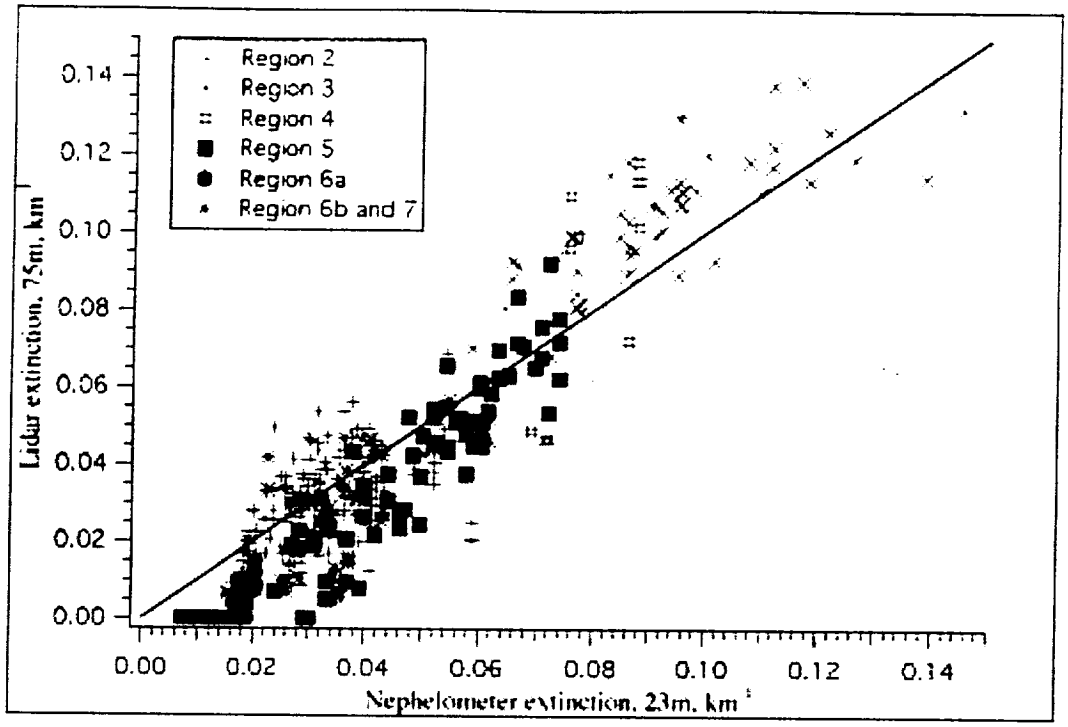
Region 2
Region 3
Region 4
Region 5
Region 6a
Region 6b and 7
Lidar extinction, 75m, km⁻¹
Nephelometer extinction, 23m, km⁻¹
0.00
0.02
0.04
0.06
0.08
0.10
0.12
0.14

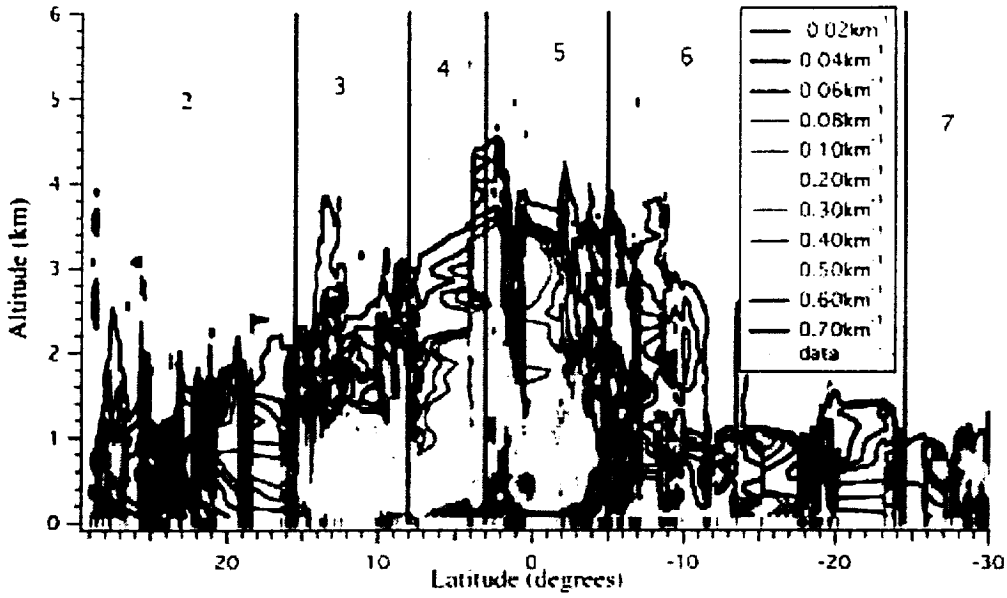
Altitude (km)
Latitude (degrees)
2
3
4
5
6
7
0.02km⁻¹
0.04km⁻¹
0.06km⁻¹
0.08km⁻¹
0.10km⁻¹
0.20km⁻¹
0.30km⁻¹
0.40km⁻¹
0.50km⁻¹
0.60km⁻¹
0.70km⁻¹
data

Figure 4

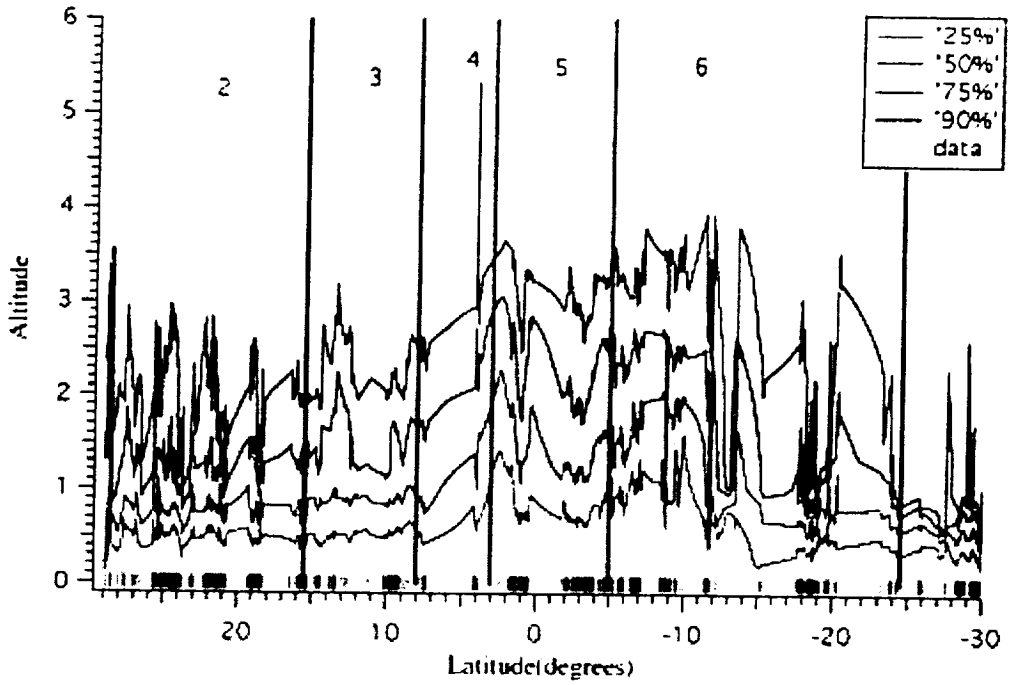
'25%'
'50%'
'75%'
'90%'
data
2
3
4
5
6
Altitude
0
1
2
3
4
5
6
20
10
0
-10
-20
-30
Latitude(degrees)

Figure 5

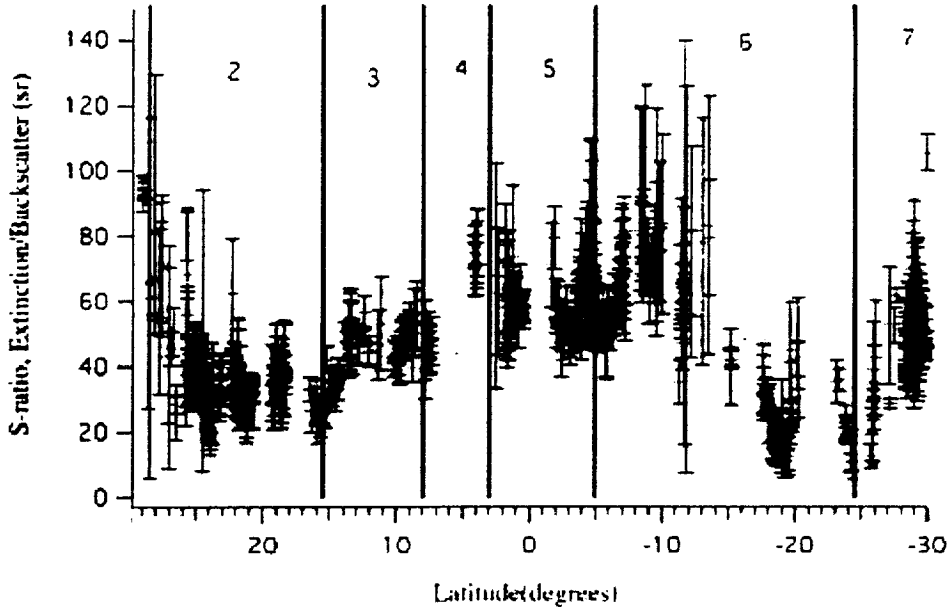
S-ratio, Extinction/Backscatter (sr)
140
120
100
80
60
40
20
0
2
3
4
5
6
7
20
10
0
-10
-20
-30
Latitude(degrees)

Figure 6

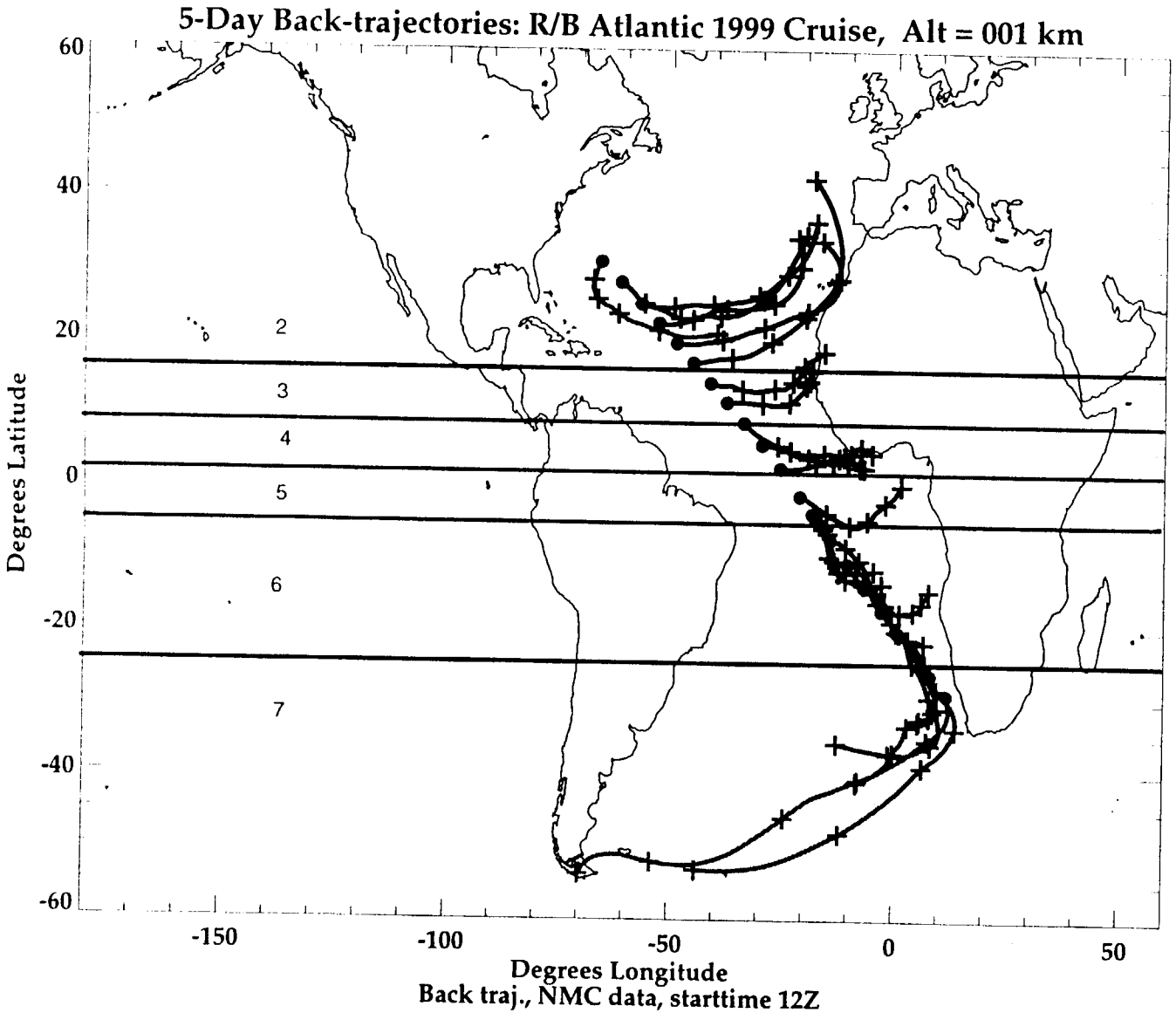
5-Day Back-trajectories: R/B Atlantic 1999 Cruise, Alt = 001 km
60
40
20
0
-20
-40
-60
Degrees Latitude
2
3
4
5
6
7
-150
-100
-50
0
50
Degrees Longitude
Back traj., NMC data, starttime 12Z

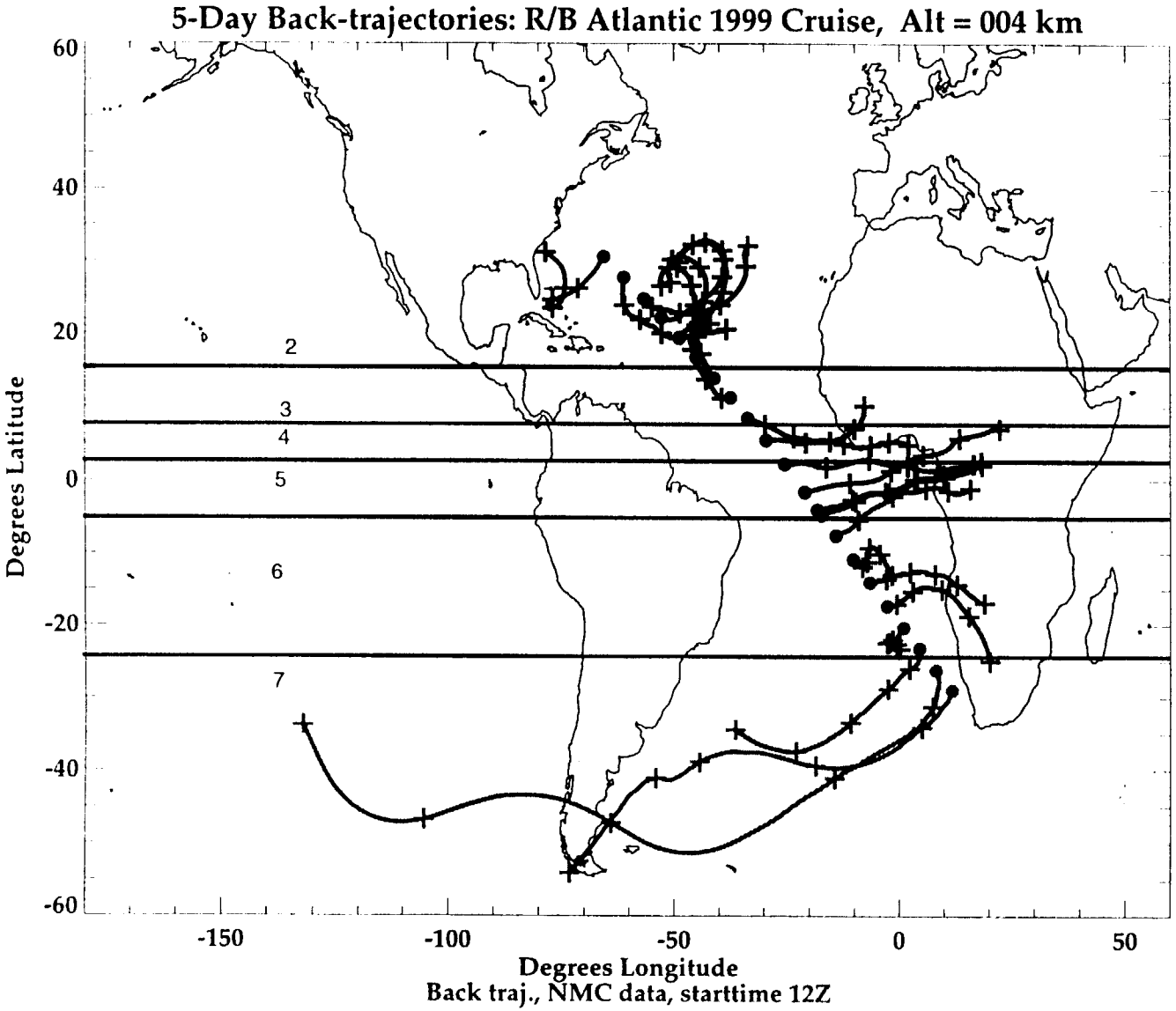
5-Day Back-trajectories: R/B Atlantic 1999 Cruise, Alt = 004 km
60
40
20
0
-20
-40
-60
Degrees Latitude
2
3
4
5
6
7
-150
-100
-50
0
50
Degrees Longitude
Back traj., NMC data, starttime 12Z

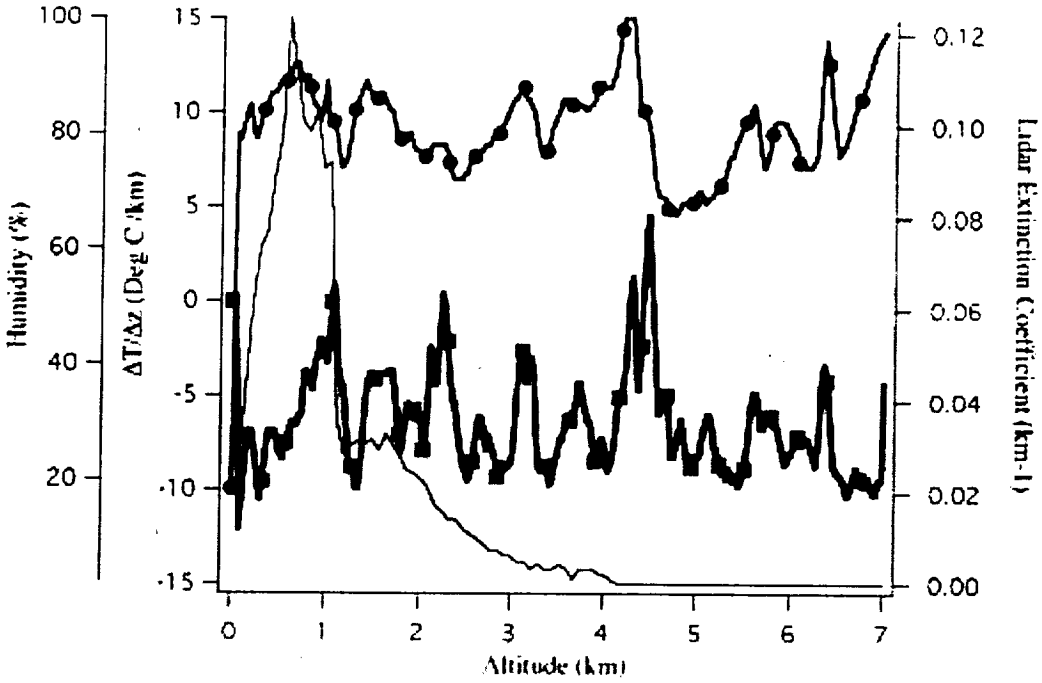
100
80
60
40
20
Humidity (%)
15
10
5
0
-5
-10
-15
ΔT/Δz (Deg C /km)
0.12
0.10
0.08
0.06
0.04
0.02
0.00
Lidar Extinction Coefficient (km-1)
0
1
2
3
4
5
6
7
Altitude (km)

Figure 9

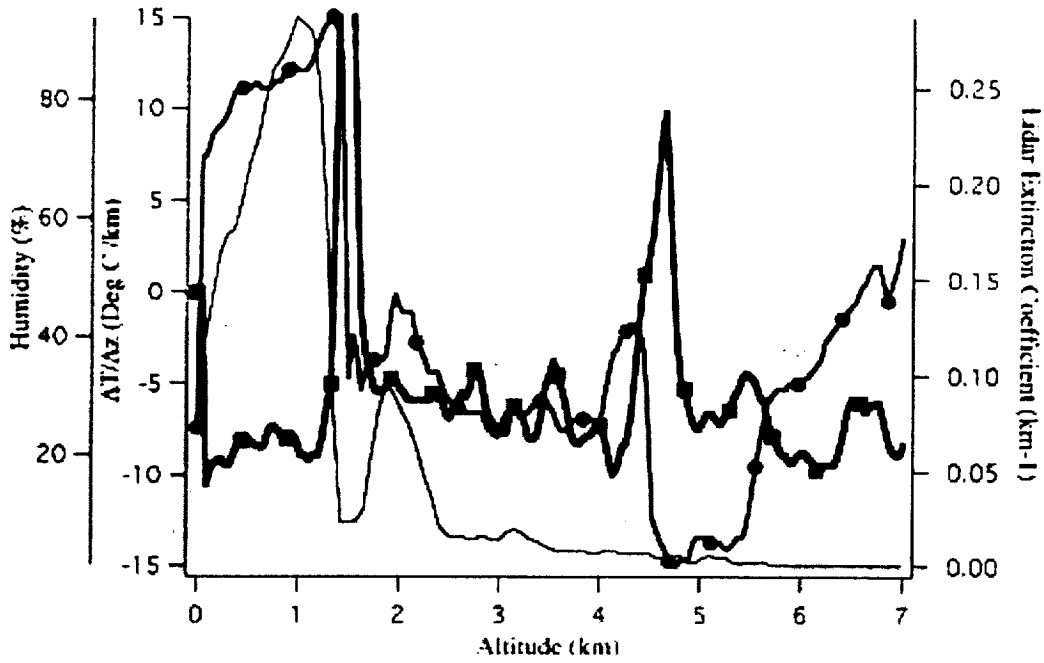
Humidity (%)
80
60
40
20
ΔT/Δz (Deg C /km)
15
10
5
0
-5
-10
-15
Lidar Extinction Coefficient (km-1)
0.25
0.20
0.15
0.10
0.05
0.00
0
1
2
3
4
5
6
7
Altitude (km)

Figure 10

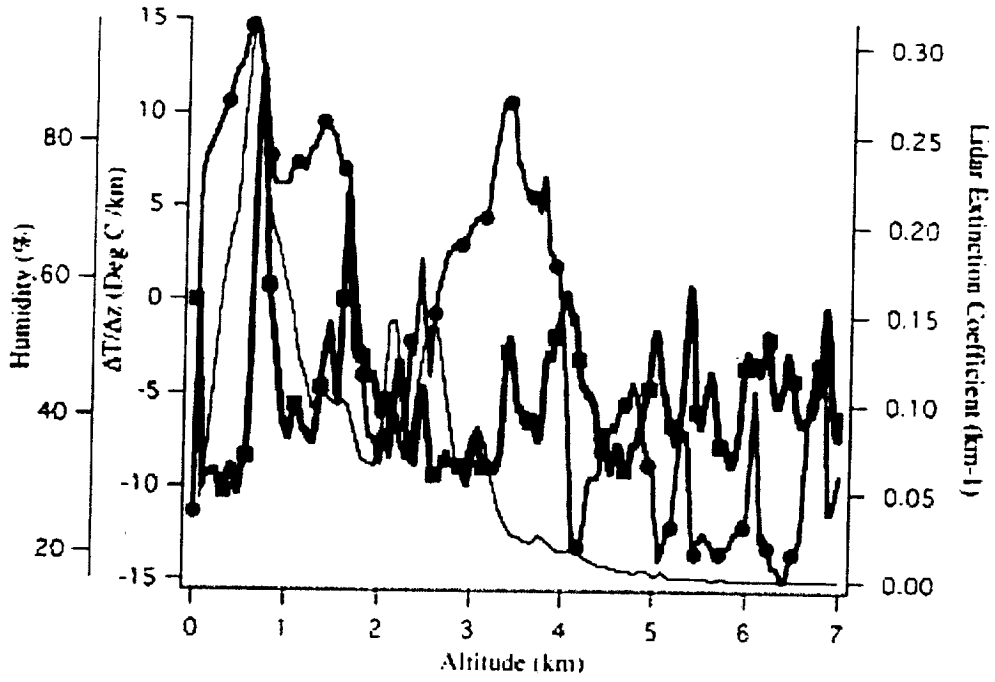
Humidity (%)
ΔT/Δz (Deg C /km)
Lidar Extinction Coefficient (km-1)
Altitude (km)
80
60
40
20
15
10
5
0
-5
-10
-15
0.30
0.25
0.20
0.15
0.10
0.05
0.00
0
1
2
3
4
5
6
7

Figure 11

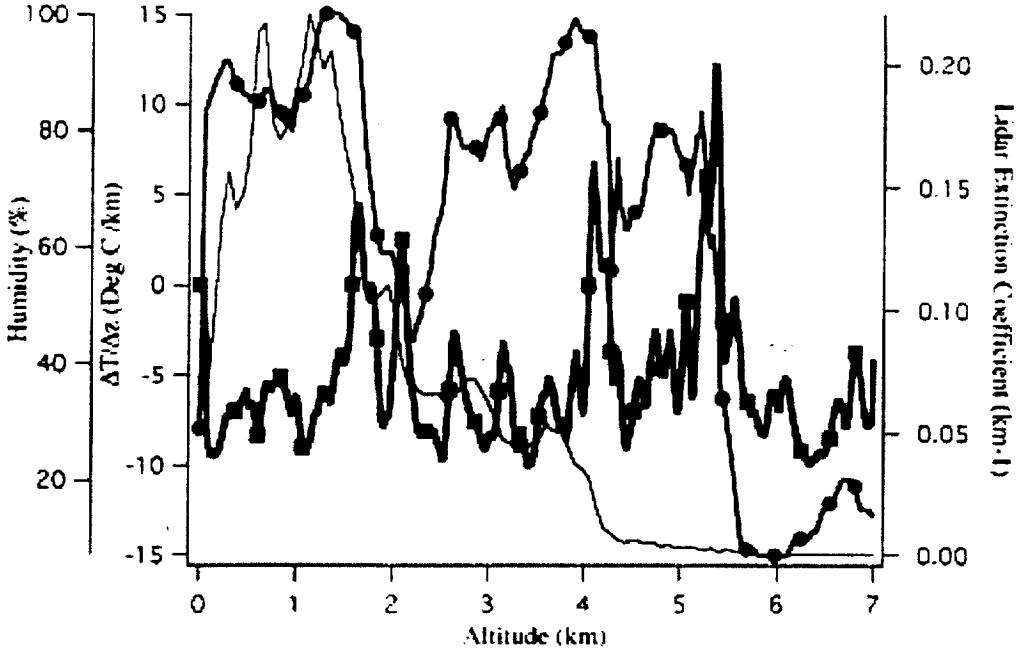
Humidity (%)
ΔT/Δz (Deg C /km)
Lidar Extinction Coefficient (km-1)
Altitude (km)
100
80
60
40
20
15
10
5
0
-5
-10
-15
0.20
0.15
0.10
0.05
0.00
0
1
2
3
4
5
6
7

Figure 12

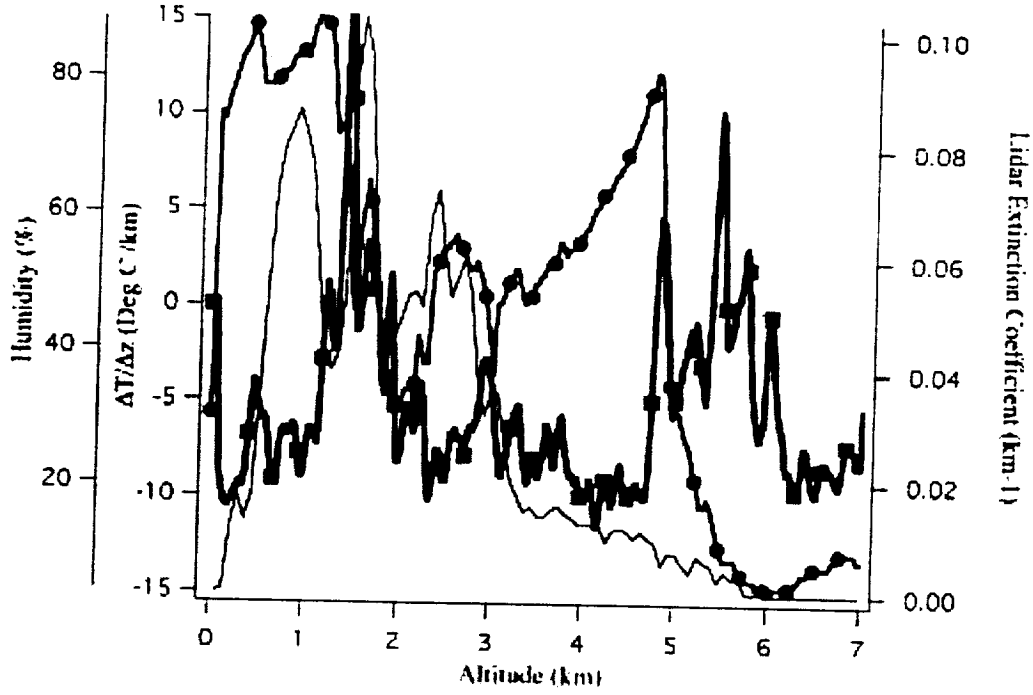
Humidity (%)
80
60
40
20
ΔT/Δz (Deg C /km)
15
10
5
0
-5
-10
-15
Lidar Extinction Coefficient (km-1)
0.10
0.08
0.06
0.04
0.02
0.00
0
1
2
3
4
5
6
7
Altitude (km)

Figure 13

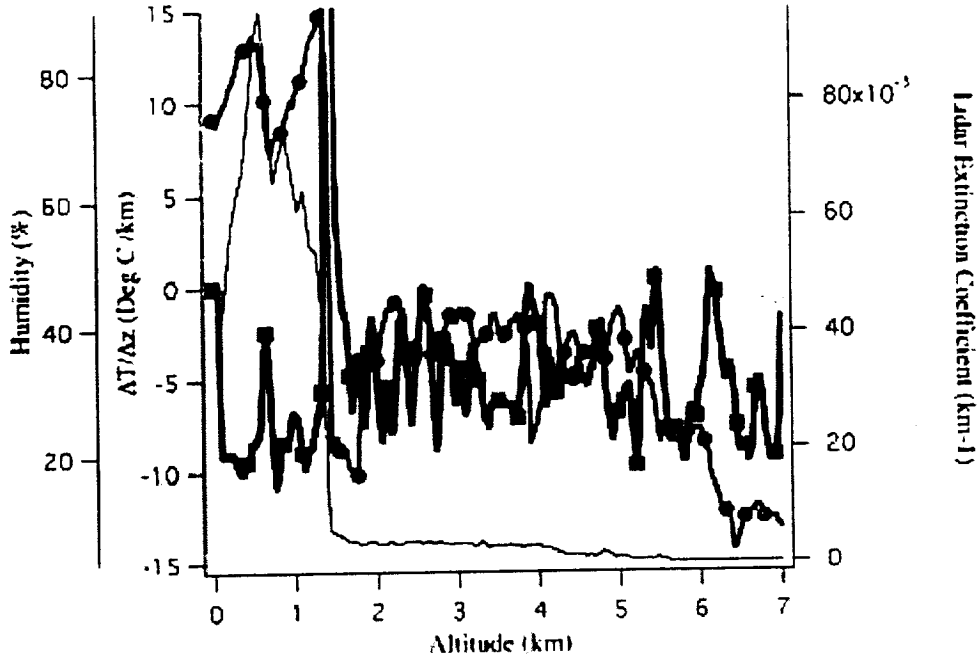
Humidity (%)
80
60
40
20
ΔT/Δz (Deg C /km)
15
10
5
0
-5
-10
-15
0
1
2
3
4
5
6
7
Altitude (km)
80x10⁻³
60
40
20
0
Lidar Extinction Coefficient (km-1)

Figure 14